LETTER

Magnetic anisotropy peculiarities of high-temperature ferromagnetic Mn_xSi_{1-x} ($x \approx 0.5$) alloy films

To cite this article: A. B. Drovosekov *et al* 2016 *EPL* **115** 37008

epl A Letters Journal Exploring the Frontiers of Physics

August 2016

EPL, **115** (2016) 37008 www.epljournal.org
doi: 10.1209/0295-5075/115/37008

Magnetic anisotropy peculiarities of high-temperature ferromagnetic Mn_xSi_{1-x} ($x \approx 0.5$) alloy films

A. B. Drovosekov[1(a)], N. M. Kreines[1], A. O. Savitsky[1], S. V. Kapelnitsky[2], V. V. Rylkov[2,3], V. V. Tugushev[2], G. V. Prutskov[2], O. A. Novodvorskii[4], E. A. Cherebilo[4], E. T. Kulatov[5], Y. Wang[6] and S. Zhou[6]

[1] *P.L. Kapitza Institute for Physical Problems RAS - Kosygina St. 2, 119334 Moscow, Russia*
[2] *National Research Centre "Kurchatov Institute" - Kurchatov Sq. 1, 123182 Moscow, Russia*
[3] *Kotel'nikov Institute of Radio Engineering and Electronics RAS - 141190 Fryazino, Moscow region, Russia*
[4] *Institute on Laser and Information Technologies RAS - Svyatoozerskaya St. 1, 140700 Shatura, Moscow region, Russia*
[5] *Prokhorov General Physics Institute RAS - Vavilov St. 38, 119991 Moscow, Russia*
[6] *Helmholtz-Zentrum Dresden-Rossendorf, Institute of Ion Beam Physics and Materials Research Bautzner Landstrasse 400, 01328 Dresden, Germany*

received 15 April 2016; accepted in final form 19 August 2016
published online 9 September 2016

PACS 75.70.-i – Magnetic properties of thin films, surfaces, and interfaces
PACS 75.30.Gw – Magnetic anisotropy
PACS 76.50.+g – Ferromagnetic, antiferromagnetic, and ferrimagnetic resonances; spin-wave resonance

Abstract – Thin films of Mn_xSi_{1-x} alloys with different Mn concentration $x \approx 0.44$–0.63 grown by the pulsed-laser deposition (PLD) method onto the Al_2O_3 (0001) substrate were investigated in the temperature range 4–300 K using ferromagnetic resonance (FMR) measurements in the wide range of frequencies ($f = 7$–60 GHz) and magnetic fields ($H = 0$–30 kOe). For samples with $x \approx 0.52$–0.55, FMR data show clear evidence of ferromagnetism (FM) with high Curie temperatures $T_C \sim 300$ K. These samples demonstrate the complex and unusual character of magnetic anisotropy described in the frame of phenomenological model as a combination of the essential second-order easy-plane anisotropy contribution and the additional fourth-order anisotropy contribution with the easy direction normal to the film plane. We explain the obtained results by a polycrystalline (mosaic) structure of the films caused by the film-substrate lattice mismatch.

Introduction. – Development of Si-Mn alloys for spintronic applications attracts a lot of attention, since these materials demonstrate unusual magnetic and transport properties and can be easily incorporated into the existing microelectronic technology [1–9].

Nonstoichiometric Mn_xSi_{1-x} alloys with high Mn content ($x \approx 0.5$, *i.e.* close to stoichiometric MnSi) seem to be particularly promising for spintronic applications. Recently we have found that in thin films of such concentrated alloys, the Curie temperature T_C increases by more than an order of magnitude as compared with bulk MnSi ($T_C \approx 30$ K) [7]. Comparative studies of anomalous Hall effect and transverse Kerr effect showed that the ferromagnetic transition in Mn_xSi_{1-x} ($x \approx 0.52$–0.55) alloys occurring at $T \sim 300$ K has a global nature and is not associated with the phase segregation [8]. Besides high T_C values, the films investigated in [7,8] show large values of saturation magnetization reaching ≈ 400 emu/cm^3 at low temperatures. The observed magnetization value corresponds to $\approx 1.1\,\mu_B$/Mn, that significantly exceeds the value $0.4\,\mu_B$/Mn typical for bulk MnSi crystal [10].

High-temperature FM in Mn_xSi_{1-x} ($x \approx 0.5$) alloys has been qualitatively interpreted [7,8] in the frame of the early proposed model for dilute Mn_xSi_{1-x} alloys [3,4], *i.e.* in terms of complex defects with local magnetic moments embedded into the matrix of itinerant FM. However, many details of FM order in Mn_xSi_{1-x} ($x \approx 0.5$) alloys are still not completely clear due to insufficient experimental studies. In particular, there are no data on their magnetic anisotropy. In the present work, thin

(a) E-mail: drovosekov@kapitza.ras.ru

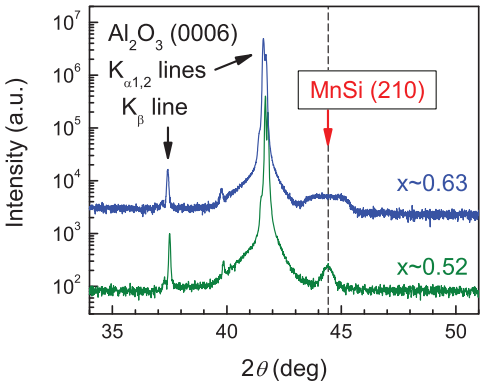

Fig. 1: (Colour online) The X-ray diffraction patterns for the Mn_xSi_{1-x}/Al_2O_3 structures with $x \approx 0.52$ and $x \approx 0.63$.

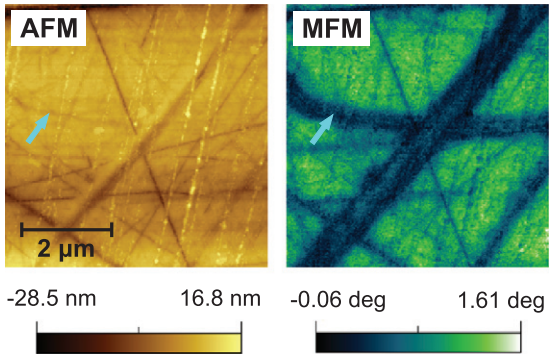

Fig. 2: (Colour online) The AFM and MFM images for the $Mn_{0.52}Si_{0.48}$ film with $T_C \approx 330$ K measured at room temperature. The light regions in the MFM image are the attracting magnetic areas. Dark regions are areas in which there is no MFM probe attraction. The arrow shows the interface between crystallites in case when it is poorly revealed in the AFM mode while it is obvious in the MFM mode.

Mn_xSi_{1-x} ($x \approx 0.52$–0.55) films are investigated by the FMR method which is powerful for providing valuable information about magnetic anisotropy peculiarities of thin-film magnetic materials (see [11] and references therein).

Samples and experimental details. – We studied six samples with manganese content in the range $x \approx 0.44$–0.63. The 70 nm thick film samples were produced by PLD method on α-$Al_2O_3(0001)$ substrates at 340 °C. The composition of the films was testified by X-ray photoelectronic spectroscopy (for details see [7]).

The structural properties of the samples were studied by X-ray diffraction (XRD) analysis using a Rigaku SmartLab diffractometer. Additionally, atomic- and magnetic force microscopy (AFM and MFM) investigations were performed at room temperature using SmartSPM (AIST-NT) microscope for the $Mn_{0.52}Si_{0.48}$ sample having the most pronounced high-T_C FM.

Static magnetization of the samples was investigated using SQUID magnetometery at $T = 4.2$–350 K.

FMR spectra were studied using a set of laboratory-developed transmission-type spectrometers at temperatures 4.2–300 K in the wide range of frequencies (f = 7–60 GHz) and magnetic fields (up to $H = 30$ kOe). Measurements were carried out for different orientations of the magnetic field with respect to the film plane.

Experimental results and discussion. –

XRD. Figure 1 demonstrates typical results of X-ray diffraction for two Mn_xSi_{1-x} films on $Al_2O_3(0001)$ substrates. In addition to strong peaks from $Al_2O_3(0006)$ the diffraction curves demonstrate a broad peak which can be attributed to the CuK_α line from ε-MnSi(210) film with B20 structure ($2\theta = 44.43°$). For the film with $x \approx 0.52$, the full width at half maximum (FWHM$_\omega$) parameter of this peak is $\Delta\omega \approx 0.4°$. Such a broad peak signifies a mosaic structure of the film and/or a high content of crystal defects in it. In particular, it may be caused by the lattice constant mismatch and different symmetries of the α-Al_2O_3 substrate (hexagonal) and ε-MnSi (cubic), as well as by the Mn excess. At increasing Mn content the ε-MnSi(210) peak transforms to a "flat hill" about 2° wide at $x \approx 0.63$ (fig. 1).

AFM and MFM. AFM and MFM studies of the sample surface confirm polycrystallinity of the film. The AFM and MFM images obtained in ambient conditions for the $Mn_{0.52}Si_{0.48}$ film are shown in fig. 2. The depth of weakly pronounced inter-block interfaces revealed in the AFM image (thin lines) does not exceed 2 nm. The strongly pronounced inter-crystallite interfaces (thick lines) have the form of cavities with the depth of < 10 nm.

For receiving the MFM images, the two-pass lift-mode technique was used. The probe attraction to the sample surface seems to arise from local reversal magnetization of the film in the field of MFM probe. Therefore, light regions on the MFM images display the areas with high local magnetic susceptibility, and dark strips show the areas where the local magnetic susceptibility is small.

Comparison of AFM and MFM images (fig. 2) shows that the positions of inter-crystallite interfaces correlate on the whole with dark strips in MFM images. This correlation can be explained by pinning of the magnetic moment at inter-crystallite boundaries.

Static magnetization. Samples with Mn concentration 0.44 and 0.63 (far from the stoichiometric value $x = 0.5$) demonstrated no FM moment at least down to 100 K [7]. On the contrary, samples with relatively small deviation from stoichiometry, $x = 0.52$–0.55, show high-temperature FM with large values of saturation magnetization (see fig. 3 and ref. [7]). Low-temperature magnetization curves demonstrate noticeable hysteresis and smooth approach to saturation (the inset in fig. 3) which can be attributed to polycrystallinity of the samples. Magnetisation measured in magnetic field applied normal to the film plane saturates at much higher fields comparing to the case of in-plane field. This fact indicates easy-plane–type magnetic anisotropy of the films.

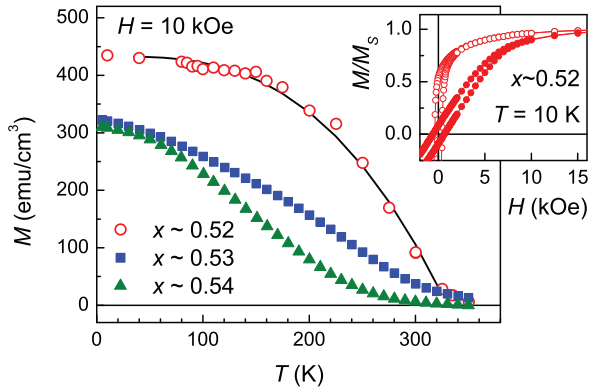

Fig. 3: (Colour online) Temperature dependence of magnetization at $H = 10$ kOe applied in the film plane for samples with different Mn concentration. The solid line is the theoretical $M(T)$ curve determined in [7] within the framework of the spin-fluctuation model [3,4]. The inset shows hysteresis loops for the $Mn_{0.52}Si_{0.48}$ film at $T = 10$ K in cases when the field is applied in the film plane (open circles) and normal to the film plane (closed circles).

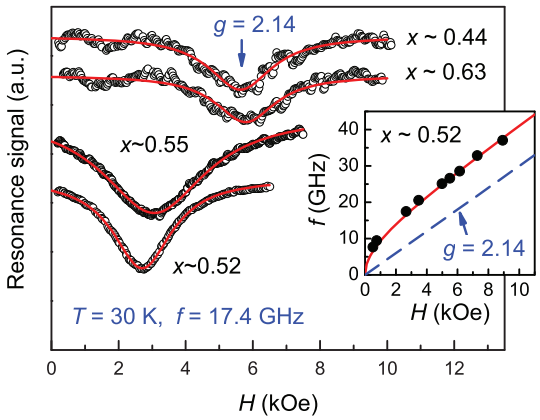

Fig. 4: (Colour online) FMR absorption signal for samples with different manganese concentration at 30 K. The magnetic field is applied in the film plane. Points are experimental data, lines are their approximation by Lorentz curve. The inset shows the experimental $f_{\|}(H)$-dependence for the $Mn_{0.52}Si_{0.48}$ sample at 30 K (points) and the result of its approximation by eq. (2) (solid line).

Ferromagnetic resonance. Resonance spectra of investigated samples demonstrate one Lorentz-shaped absorption peak (fig. 4). The resonance line position does not depend on the in-plane orientation of the external field. This result is obvious, considering the polycrystalline structure of the films.

For films with Mn concentration $x \approx 0.44$ and $x \approx 0.63$, the resonance peak is weak and its position corresponds to a paramagnetic resonance situation, *i.e.* $f = \gamma H$, with the gyromagnetic ratio $\gamma \approx 3.0$ GHz/kOe (Landé g-factor value $g = 2.14$), which is in agreement with the value reported in ref. [12] for bulk MnSi single crystal. Paramagnetism of the samples with $x \approx 0.44$ and $x \approx 0.63$ is observed in the temperature range 20–300 K, that is in accordance with the results of ref. [7].

At low temperatures, in case when magnetic field is applied in the film plane, samples with $x \approx 0.52$–0.55 show much stronger absorption peak shifted to the region of smaller fields with respect to paramagnetic samples (fig. 4). The observed shift is typical for FMR in thin films. It is connected with significant demagnetizing field and/or easy-plane anisotropy in the FM film. To describe phenomenologically the position of the FMR line we consider uniaxial magnetic anisotropy of the sample with symmetry axis normal to the film plane. The energy of such anisotropy can be written in the form [13,14]

$$E_A = K_1 \cos^2\theta + K_2 \cos^4\theta, \qquad (1)$$

where $\cos\theta = M_z/M$ is the direction cosine of magnetization vector $\boldsymbol{M}$ (M_z is its component normal to the film plane), K_1 and K_2 are anisotropy constants of the second and fourth order, respectively. It may be noticed that the angular dependence given by the second term in eq. (1) can be written in the form $K_2 \cos^2\theta + (K_2/8)\cos 4\theta$. Formally, this dependence contains a higher symmetry (biaxial anisotropy) term additional to the uniaxial anisotropy term. However, this higher symmetry contribution can prevail only in the case $K_2 \sim -K_1$ which is not realized in our system (see table 1).

Table 1: Demagnetizing field and anisotropy parameters for samples with Mn content $x \approx 0.52$, 0.53 at $T = 4.2$ K.

x	$4\pi M$	$K_{\|}M$ (kOe)	$K_{\perp}M$	K_1 (10^6 erg/cm^3)	K_2 (10^6 erg/cm^3)
0.52	5.5	9.0	6.4	0.8	−0.3
0.53	4.1	10.8	8.7	1.1	−0.2

When the magnetic field is applied in the film plane, FMR frequency $f_{\|}$ is given by [13–15]

$$f_{\|} = \gamma\sqrt{H(H + K_{\|}M)}, \qquad (2)$$

where $K_{\|}M = 4\pi M + 2K_1/M$. Equation (2) explains the observed shift of the FMR line for FM samples ($x \approx 0.52$–0.55) by large $K_{\|}M$ value. The experimental $f_{\|}(H)$-dependences can be good approximated by eq. (2) (see inset in fig. 4). A weak deviation of experimental points from the calculated $f_{\|}(H)$ curve is observed only in the region of lowest fields at frequencies $f \lesssim 10$ GHz where the domain structure of samples seems to play an important role and the phenomenological formula (2) becomes inapplicable.

Figure 5 shows experimentally determined temperature dependences of the $K_{\|}M$ parameter for all studied samples. The shape of $K_{\|}M(T)$ curves repeats qualitatively the static $M(T)$-dependences (fig. 3). Thus FMR data confirm the presence of high-T_C ferromagnetism in

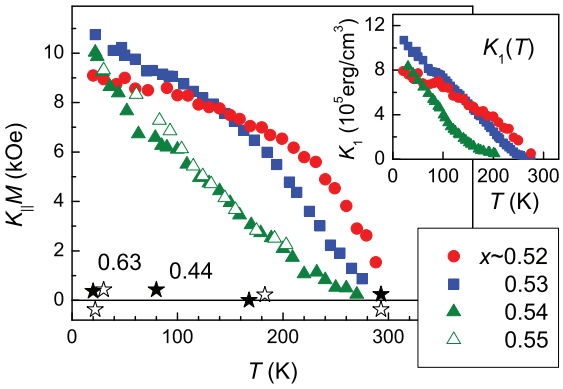

Fig. 5: (Colour online) Experimental temperature dependence of the $K_{\|}M$ parameter (see eq. (2)) for samples with different Mn concentration. The inset shows resulting temperature dependence of the anisotropy constant K_1 for samples with $x \approx 0.52$–0.54.

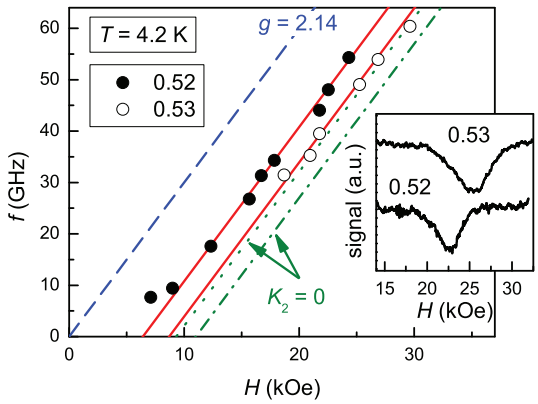

Fig. 6: (Colour online) Dependence of the resonance frequency on the magnetic field applied normal to the film plane for samples with $x \approx 0.52$, 0.53 at $T = 4.2$ K. Points are experimental data; solid lines are the theoretical curves according to eq. (3). The dotted and dash-dotted lines would correspond to the samples with $x \approx 0.52$ and $x \approx 0.53$ respectively, if we considered $K_{\perp}M = K_{\|}M$. The inset demonstrates examples of the experimental resonance spectra at frequency ≈ 49 GHz.

the investigated films with $x \approx 0.52$–0.55. Moreover, for all these samples the observed $K_{\|}M$ values exceed considerably (about 2 times) the static demagnetization fields $4\pi M$. This fact indicates large magnetic easy-plane anisotropy of the films. The corresponding temperature dependences of K_1 constant are shown in the inset of fig. 5.

To obtain further insight into peculiarities of the magnetic anisotropy of our system, the $f(H)$-dependences were investigated for samples with $x \approx 0.52$ and $x \approx 0.53$ at $T = 4.2$ K, when the applied field was perpendicular to the film plane (fig. 6). In this case the calculated FMR frequency $f_{\perp}$ in the saturation regime has a linear dependence on the applied external field [13–15]:

$$f_{\perp} = \gamma(H - K_{\perp}M), \tag{3}$$

where $K_{\perp}M = K_{\|}M + 4K_2/M$.

In agreement with eq. (3), the experimental $f_{\perp}(H)$-dependences are linear in the region of high frequencies and fields (fig. 6). However, the observed $K_{\perp}M$ values prove to be noticeably less than low temperature values for the $K_{\|}M$ parameter (table 1). Within our approach this fact is explained by additional fourth-order anisotropy of the films with negative sign of K_2 constant (easy direction normal to the film plane).

As an additional demonstration of the role of K_1 and K_2 anisotropy constants in the investigated films, we measured the out-of-plane angular dependence of resonance field in $Mn_{0.52}Si_{0.48}$ sample (fig. 7). When the magnetic field is oriented at an angle θ_H with respect to the axis **z** normal to the film plane, the resonance frequency f is defined by the equation (similar to that in [14]):

$$\frac{f^2}{\gamma^2} = \{H\cos(\theta - \theta_H) - H_A\cos^2\theta\} \times \left\{H\cos(\theta - \theta_H) - H_A\cos 2\theta + \frac{K_2}{M}(1 - \cos 4\theta)\right\}, \tag{4}$$

where $H_A = K_{\|}M + 4K_2/M\cos^2\theta$. The angle θ defines the static orientation of the magnetization vector. It can be determined from the total energy minimization which leads to the equation (similar to that in [14]):

$$H\sin(\theta - \theta_H) = H_A\cos\theta\sin\theta. \tag{5}$$

Solving the system of eqs. (4), (5) at given frequency, the angular dependence of the resonance field $H_{\rm res}(\theta_H)$ can be obtained. The correspondence between the resulting theoretical curve and the experimental data is not perfect (fig. 7), though the agreement is much better if the fourth-order anisotropy constant K_2 is taken into account. The observed discrepancy is probably due to limited applicability of the proposed theoretical approach. The considered phenomenological model treats the film as a homogeneous one, while the real sample is polycrystalline.

Possible origin of magnetic anisotropy. The single-crystal itinerant ferromagnet MnSi with B20 structure has a weak fourth-order cubic magnetic anisotropy. But in the case of a thin epitaxial MnSi film deposited on a substrate, the induced uniaxial magnetic anisotropy can be large due to mechanical deformations of the crystal caused by lattice mismatch between the film and the substrate (see [16] and references therein).

In our case, sufficiently large mismatch ($\approx 10\%$) between the Al_2O_3 substrate and Mn_xSi_{1-x} film can be realized. Indeed, the symmetry of the α-$Al_2O_3(0001)$ substrate is sixfold which leads to the preferable [111] growth direction of the cubic Mn_xSi_{1-x} crystal. Comparing the distance between $(1120)_{\alpha-Al_2O_3}$ atomic planes ($d = 2.38$ Å) with that between $(111)_{\rm MnSi}$ planes ($d = 2.63$ Å), the lattice mismatch is estimated as 10%, which is huge [17]. It is one of the main reasons for polycrystallinity of the grown film and thus initiates an existence

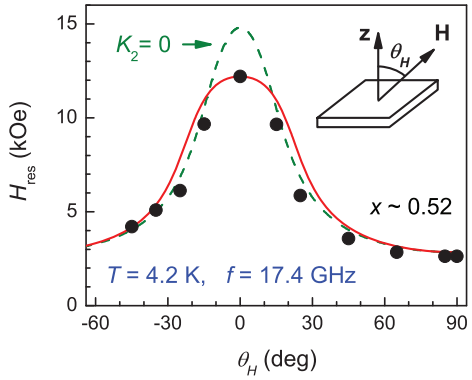

Fig. 7: (Colour online) Out-of-plane angular dependence of the resonance field in $Mn_{0.52}Si_{0.48}$ sample ($T = 4.2$ K, $f = 17.4$ GHz). Points are experimental data; lines are theoretical calculations in cases when the K_2 coefficient is taken into account (solid line) and when K_2 is neglected (dashed line). The experimental geometry is shown in the plot.

of inter-crystallite and crystallite-substrate strain, producing crystal twin planes or inter-crystallite boundaries [18].

Comparing the results of XRD and AFM-MFM measurements, we suppose that the grown Mn_xSi_{1-x} films are textured or mosaic type with the typical size of crystallite about 1 μm. Obviously, in the frame of the used methods we are unable to adduce direct experimental proofs of the strain inside our films; so, our supposal should be verified in future studies. However, it is well known that mechanical stress on the inter-crystallite boundaries can induce elastic or plastic deformation (even dislocation) near these boundaries [18]. Following this paradigm, at least a part of thin lines in the AFM images (one of them is indicated in fig. 2 by the arrow) may be associated with the projections of inter-crystallite interfaces on the film surface.

In this case, the MFM data shed light on the magnetic structure of the film surface. The MFM signal is locally dark (weak magnetic susceptibility) nearby the lines corresponding to projections of inter-crystallite interfaces. A possible reason for such an effect is due to the significant enhancement of magnetic anisotropy near the inter-crystallite boundaries. This enhancement may be provided by an increase of anisotropic (for example, spin-orbit) component of effective exchange coupling between local magnetic moments of Mn-containing nanometer scale defects, due to strong crystal potential distortions near the inter-crystallite boundaries. Following our supposition, the "local" axes of magnetic anisotropy are oriented normally to the inter-crystallite interfaces, *i.e.* lie for the most part in the film plane. These interfaces are randomly distributed in the film, they strongly pin local magnetic moments of Mn-containing defects and block a local reversal magnetization in MFM measurements.

At the same time, randomly distributed "local" in-plane axes of magnetic anisotropy lead to existence of effective "global" uniaxial anisotropy with symmetry axis normal to the film plane. This anisotropy becomes apparent in FMR experiments.

For a qualitative understanding of the possible microscopic mechanism of magnetic anisotropy in our system, let us discuss the early proposed simple quantum mechanical model of randomly distributed crystallites having additional spin-orbit coupling with the matrix of a weak itinerant ferromagnet due to the inter-crystallite boundaries, which enhances magnetic anisotropy [19]. It seems that within this model, we can at least qualitatively support the phenomenological approach to the FMR description. In particular, the model predicts the essential second-order easy-plane anisotropy contribution with $K_1 > 0$ and the additional fourth-order anisotropy contribution with $K_2 < 0$. However, the ratio $|K_2|/K_1$ estimated from the model [19] is $|K_2|/K_1 \sim 10^{-3}$–10^{-4}, that is much less than the value $|K_2|/K_1 \sim 0.2$–0.4 found from our experiment (see table 1). One possible reason of this disagreement is the used in [19] perturbation approach to the spin-orbit coupling in the conventional spin-fluctuation theory [20] for a weak itinerant ferromagnet, while in Si-Mn alloys such approach may be not well justified. On the other hand, the crystallite-substrate strain which can enhance the spin-orbit effects in real alloys, is completely neglected in [19].

At the same time, it should be kept in mind that the phenomenological description of FMR is developed for a purely homogeneous case, *i.e.* it does not consider the distribution of local anisotropy in the plane and on the film thickness. Therefore, the constants K_1 and K_2 found with its help have only an efficient character.

Conclusions. – In this work, for thin films of nonstoichiometric Mn_xSi_{1-x} alloys with Mn content $x \approx 0.52$–0.55, the FMR data confirmed the early reported FM order with high Curie temperatures $T_C \sim 300$ K [7,8].

Further to the fact of FM order itself, the studied samples also demonstrated in FMR measurements an intricate character of magnetic anisotropy, which can be described in a phenomenological way as a combination of two contributions: the second-order easy-plane anisotropy component and the fourth-order anisotropy component with easy direction normal to the film plane. We attribute this magnetic anisotropy to the existence of a mosaic (polycrystalline) structure of the films. We believe that such a structure is revealed in presented structural measurements, accompanied by the strain between crystallites and/or crystallites-substrate. According to our assumption, the strain can initiate an enhancement of the spin-orbital anisotropic component of exchange interaction between the local moment of magnetic defects and itinerant electron spins. This enhancement becomes apparent as a pinning of local magnetic moments in the MFM images.

We hope that the combination of FMR, XRD, AFM and MFM methods showed its efficiency in the study of nonstoichiometric Mn_xSi_{1-x} alloys as a new class of high-temperature FM semiconductor materials.

* * *

We are grateful to V. Glazkov (IPP RAS) for assistance in carrying out FMR measurements in the region of high fields. We express our gratitude to A. Temiryazev (IRE RAS) for AFM and MFM measurements. We would also like to thank him as well as D. Kholin (IPP RAS) and E. Pashaev (NRC "Kurchatov Institute") for fruitful discussions of FMR and XRD results. The work was partly supported by the RSF (grant No. 16-19-10233) and RFBR (grant Nos. 15-07-01170, 14-07-91332, 14-07-00688, 15-29-01171, 14-47-03605, 15-07-04142). The work at HZDR is financially supported by DFG (ZH 225/6-1).

REFERENCES

[1] Zhou S. and Schmidt H., *Materials*, **3** (2010) 5054.
[2] Zhou S., Potzger K., Zhang G., Mücklich A., Eichhorn F., Schell N., Grötzschel R., Schmidt B., Skorupa W., Helm M., Fassbender J. and Geiger D., *Phys. Rev. B*, **75** (2007) 085203.
[3] Men'shov V. N., Tugushev V. V. and Caprara S., *Phys. Rev. B*, **83** (2011) 035201.
[4] Men'shov V. N. and Tugushev V. V., *J. Exp. Theor. Phys.*, **113** (2011) 121.
[5] Kahwaji S., Gordon R. A., Crozier E. D., Roorda S., Robertson M. D., Zhu J. and Monchesky T. L., *Phys. Rev. B*, **88** (2013) 174419.
[6] Demidov E. S., Podol'skii V. V., Lesnikov V. P., Pavlova E. D., Bobrov A. I., Karzanov V. V., Malekhonova N. V. and Tronov A. A., *JETP Lett.*, **100** (2015) 719.
[7] Rylkov V. V., Nikolaev S. N., Chernoglazov K. Yu., Aronzon B. A., Maslakov K. I., Tugushev V. V., Kulatov E. T., Likhachev I. A., Pashaev E. M., Semisalova A. S., Perov N. S., Granovskii A. B., Gan'shina E. A., Novodvorskii O. A., Khramova O. D., Khaidukov E. V. and Panchenko V. Ya., *JETP Lett.*, **96** (2012) 255.
[8] Rylkov V. V., Gan'shina E. A., Novodvorskii O. A., Nikolaev S. N., Novikov A. I., Kulatov E. T., Tugushev V. V., Granovskii A. B. and Panchenko V. Ya., *EPL*, **103** (2013) 57014.
[9] Yang A., Zhang K., Yan S., Kang S., Qin Y., Pei J., He L., Li H., Dai Y., Xiao S. and Tian Y., *J. Alloys Compd.*, **623** (2015) 438.
[10] Stishov S. M. and Petrova A. E., *Phys. Usp.*, **54** (2011) 1117.
[11] Hagmann J. A., Traudt K., Zhou Y. Y., Liu X., Dobrowolska M. and Furdyna J. K., *J. Magn. & Magn. Mater.*, **360** (2014) 137.
[12] Demishev S. V., Glushkov V. V., Lobanova I. I., Anisimov M. A., Ivanov V. Yu., Ishchenko T. V., Karasev M. S., Samarin N. A., Sluchanko N. E., Zimin V. M. and Semeno A. V., *Phys. Rev. B*, **85** (2012) 045131.
[13] Vonsovskii S. V., *Ferromagnetic Resonance* (Pergamon Press, Oxford) 1966.
[14] Zhang Y., Yan S. S., Liu Y. H., Tian Y., Liu G., Chen Y., Mei L. and Liu J. P., *Solid State Commun.*, **140** (2006) 405.
[15] Kittel C., *J. Phys. Radium*, **12** (1951) 291.
[16] Wilson M. N., Butenko A. B., Bogdanov A. N. and Monchesky T. L., *Phys. Rev. B*, **89** (2014) 094411.
[17] Nikolaev S. N., Semisalova A. S., Rylkov V. V., Tugushev V. V., Zenkevich A. V., Vasiliev A. L., Pashaev E. M., Chernoglazov K. Yu., Chesnokov Yu. M., Likhachev I. A., Perov N. S., Matveyev Yu. A., Novodvorskii O. A., Kulatov E. T., Bugaev A. S., Wang Y. and Zhou S., *AIP Adv.*, **6** (2016) 015020.
[18] Kosevich A. M. and Boiko V. S., *Sov. Phys. Usp.*, **14** (1971) 286.
[19] Drovosekov A. B., Kreines N. M., Savitsky A. O., Kapelnitsky S. V., Rylkov V. V., Tugushev V. V., Prutskov G. V., Novodvorskii O. A., Shorokhova A. V., Wang Y. and Zhou S., arXiv:1510.02634 [cond-mat.mtrl-sci].
[20] Moriya T., *Spin Fluctuations in Itinerant Electron Magnetism* (Springer-Verlag, Berlin) 1985.